Function and expression of the epithelial Ca^{2+} channel family: comparison of mammalian ECaC1 and 2

Hoenderop JGJ, Vennekens R, **Müller D**, Prenen J, Droogmans G, Bindels RJM, Nilius B

J Physiol(London) 2001, 537: 747-761

Function and expression of the epithelial Ca^{2+} channel family: comparison of mammalian ECaC1 and 2

Joost G. J. Hoenderop, Rudi Vennekens*, Dominik Müller, Jean Prenen*, Guy Droogmans*, René J. M. Bindels and Bernd Nilius*

*Department of Cell Physiology, Institute of Cellular Signalling, University Medical Centre Nijmegen, The Netherlands and *Department of Physiology, Campus Gasthuisberg, KU Leuven, Belgium*

(Resubmitted 28 June 2001; accepted after revision 6 September 2001)

1. The epithelial Ca^{2+} channel (ECaC) family represents a unique group of Ca^{2+}-selective channels that share limited homology to the ligand-gated capsaicin receptors, the osmolarity-sensitive channel OTRPC4, as well as the transient receptor potential family. Southern blot analysis demonstrated that this family is restricted to two members, ECaC1 and ECaC2 (also named CaT1).

2. RT-PCR analysis demonstrated that the two channels are co-expressed in calbindin-D-containing epithelia, including small intestine, pancreas and placenta, whereas kidney and brain only express ECaC1 and stomach solely ECaC2.

3. From an electrophysiological point of view, ECaC1 and ECaC2 are highly similar channels. Differences concern divalent cation permeability, the kinetics of Ca^{2+}-dependent inactivation and recovery from inactivation.

4. Ruthenium red is a potent blocker of ECaC activity. Interestingly, ECaC2 has a 100-fold lower affinity for ruthenium red (IC_{50} 9 ± 1 μM) than ECaC1 (IC_{50} 121 ± 13 nM).

5. ECaCs are modulated by intracellular Mg^{2+} and ATP. ECaC1 and ECaC2 activity rapidly decay in the absence of intracellular ATP. This effect is further accelerated at higher intracellular Mg^{2+} concentrations.

6. In conclusion, ECaC1 and ECaC2 are homologous channels, with an almost identical pore region. They can be discriminated by their sensitivity for ruthenium red and show differences in Ca^{2+}-dependent regulation.

Cation channels are involved in a large variety of important cellular functions, such as molecular transduction of painful stimuli, osmo-regulation, capacitative Ca^{2+} entry and transepithelial ion transport (Caterina *et al.* 1997; Peng *et al.* 1999; Hoenderop *et al.* 1999*a*, 2000*b*; Liedtke *et al.* 2000). Distinctive members of this fast growing family of ion channels include vanilloid receptors, transient receptor potential (TRP) channels and epithelial Ca^{2+} channels (ECaCs). In general, the functional characterization of these channels has shed light on new physiological mechanisms.

In particular, the recent cloning and characterization of ECaC1 has identified the rate-limiting Ca^{2+} entry step responsible for transepithelial Ca^{2+} transport in kidney and small intestine (Hoenderop *et al.* 1999*a*). This family of epithelial Ca^{2+} channels includes ECaC1 and calcium transporter 1 (CaT1 or ECaC2) (Peng *et al.* 1999; Barley *et al.* 2001). These channels are highly homologous and consist of six transmembrane domains, including a putative pore-forming region between transmembrane segments 5 and 6 (Hoenderop *et al.* 1999*a*, 2000*b*). Genomic analysis showed that human ECaC1 and ECaC2 originate from two genes juxtaposed on chromosome 7q35 (Müller *et al.* 2000*a*). ECaC shares its topology with other cation channels, including vanilloid receptors and TRP channels, but also the *Shaker* potassium channel (Hoenderop *et al.* 2000*a*,*b*).

ECaC1 has recently been analysed in electrophysiological studies using *Xenopus laevis* oocytes and human embryonic kidney (HEK) 293 cells heterologously expressing ECaC1 (Hoenderop *et al.* 1999*b*; Vennekens *et al.* 2000, 2001*a*,*b*; Nilius *et al.* 2000, 2001*a*,*c*). The current through this constitutively activate channel is Ca^{2+} selective with a substantial permeability at physiological membrane potentials and a Ca^{2+}-dependent feedback regulation including fast inactivation and a slow decay (Vennekens *et al.* 2000). In contrast, the electrophysiological properties of ECaC2 have been mainly

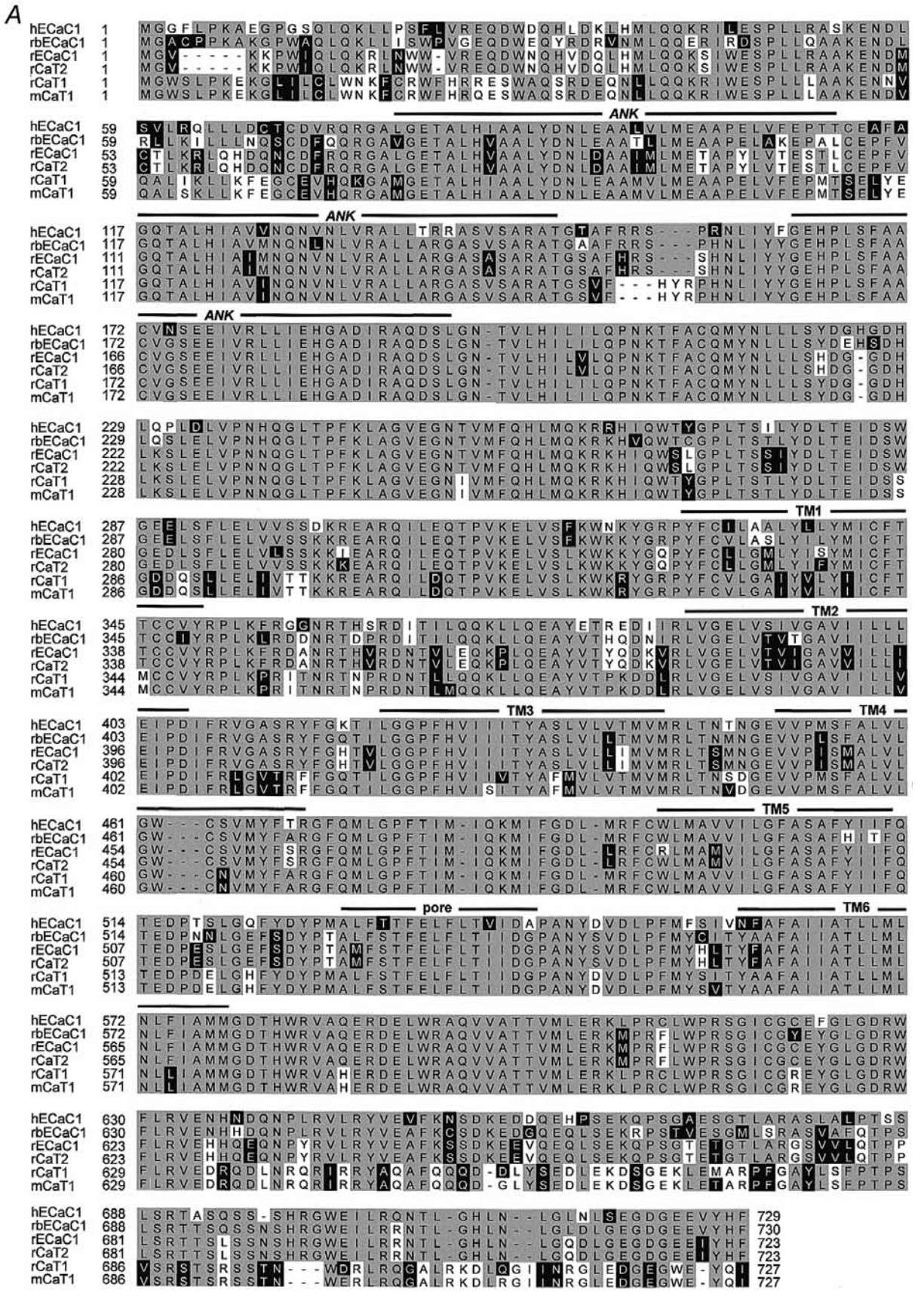

Figure 1. Phylogenetic analysis of the ECaC family

A, multiple alignment of amino acid sequence of hECaC1 (GenBank accession no. AJ271207), rbECaC1 (AJ133128), rECaC1 (AB032019), rCaT2 (AF209196), rCaT1 (AF160798) and mCaT1 (AB037373). Identical

investigated in *Xenopus laevis* oocytes by voltage-clamp analysis (Peng *et al.* 1999) and recently by patch-clamp analysis in Chinese hamster ovary cells (Suzuki *et al.* 2000; Yue *et al.* 2001).

The aim of the present study was, therefore, to characterize ECaC2 in more detail and to compare its properties with those of ECaC1 to obtain a better understanding of transcellular Ca^{2+} transport in epithelia. To this end, various aspects of these epithelial Ca^{2+} channels were studied, including the expression profile at the mRNA level by RT-PCR and the permeation and gating properties by patch-clamp analysis.

METHODS

Construction of mammalian expression vectors

The entire open reading frame from mouse ECaC2 was sub-cloned as an *Eco*R I fragment from pSPORT-mECaC2 (Suzuki *et al.* 2000) into the pCINeo/IRES-BFP vector (Trouet *et al.* 1997). This bicistronic expression vector pCINeo/IRES-BFP/mECaC2 was used to co-express mECaC2 and blue fluorescent protein (BFP). The entire open reading frame from rabbit ECaC1 (rbECaC1) was sub-cloned as a *Pvu* II–*Bam*H I fragment into the pCINeo/IRES-GFP vector as described previously (Vennekens *et al.* 2000).

Tissue distribution

The expression pattern of ECaC1 and ECaC2 was investigated by screening various human tissues, including spleen, prostate, testis, ovary, skeletal muscle, placenta, pancreas, lung, liver, kidney, heart, brain, oesophagus, stomach, duodenum, jejunum, ileum, ileocaecum, colon ascendens, colon transversum, colon descendens and rectum. These cDNA samples were purchased from Clontech (Palo Alto, CA, USA). Primers for ECaC1 (forward 5′-GGGGACCGCTGGTTCCTG-CGG-3′ and reverse 5′-TCAAAAATGGTAGACCTCCTCTCC-3′, amplified DNA product was 312 bp) and ECaC2 (forward 5′-GGG-GACCGCTGGTTCCTGCGG-3′ and reverse 5′-AGATCTGATATTC-CCAGCTCT-3′, amplified DNA product was 301 bp) were designed based on results obtained by rapid amplification of cDNA ends (RACE), as described previously (Müller *et al.* 2000*a*). To avoid false positive results due to genomic contamination of the samples, the primers spanned an intron at the genomic level. PCRs were performed in a volume of 50 μl using 50 ng cDNA of each tissue, 10 pmol of each primer, 10 mM Tris-HCl (pH 8.3), 50 mM KCl, 1.5 mM $MgCl_2$, 0.2 mM dNTP mix and 1 unit *Taq* polymerase (Gibco BRL). After an initial step for 1 min at 95 °C, amplification was performed for 33 cycles at 94 °C for 30 s followed by 60 °C for 1 min and 68 °C for 1 min. The integrity of the cDNA from various tissues was confirmed by the presence of the house-keeping gene glyceraldehyde 3-phosphate dehydrogenase (GAPDH) (forward 5′-GCAACTGCAGGA-AGAGCAAGAAATGCA-3′ and reverse 5′-TGGCACGGCCATAAG-AGGTAGATGTCA-3′, amplified DNA product was 1.2 kb). PCR conditions were as described above. Samples were analysed on a 1.4 % ethidium bromide-stained agarose gel.

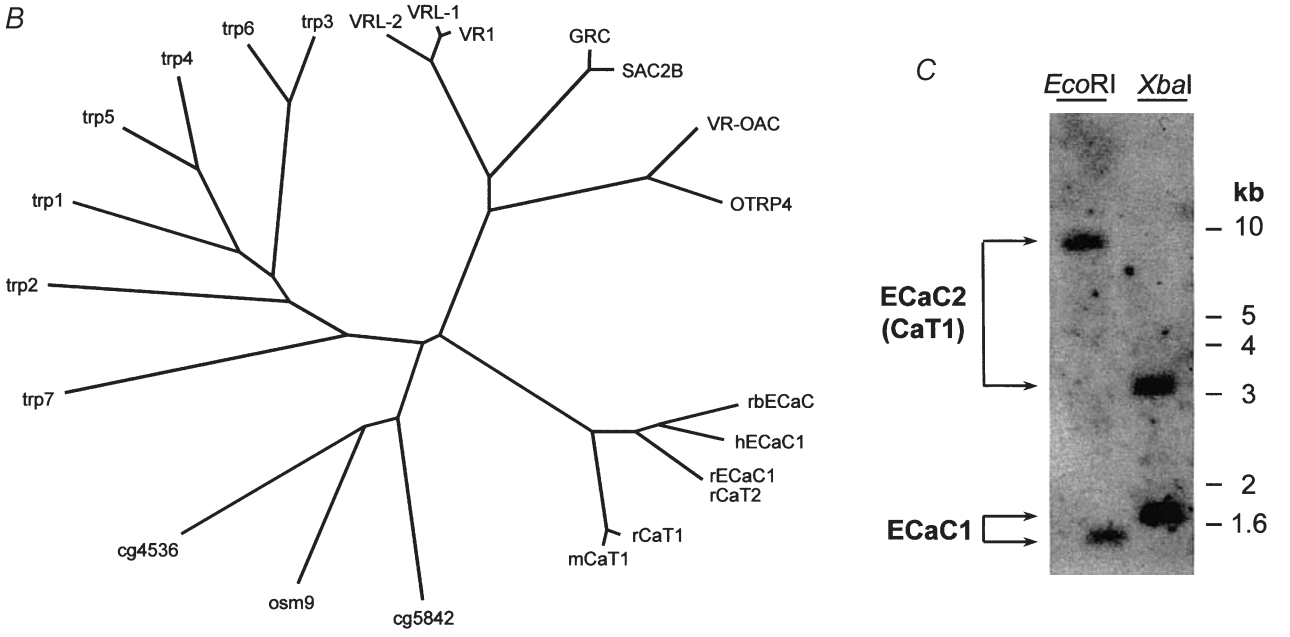

amino acids are indicated in grey, conserved amino acids in black and non-conserved amino acids in white boxes. Putative transmembrane segments (TM), the putative pore region and predicted ankyrin repeats (ANK) are indicated by bars. *B*, phylogram based on full-length amino acid sequences of trp1 (NM003304), trp2 (AF136401), trp3 (NM003305), trp4 (AF175406), trp5 (XM010296), trp6 (NM004621), trp7 (NM003307), cg4536 (AE003438), cg5842 (AE003535), osm9 (AF031408), VR1 (AJ277028), VRL-1 (NM016113), VRL-2 (Delany *et al.* 2001), GRC (AB021665), SAC2B (AB029330), VR-OAC (AF26523), OTRP4 (NM022017), rbECaC (AJ133128), hECaC1 (AJ271207), rECaC1 (AB032019), rCaT2 (AF209196), rCaT1 (AF160798) and mCaT1 (AB037373). *C*, Southern blot analysis of mouse genomic DNA digested by *Xba*I or *Eco*R I and subsequently probed with a cDNA probe containing the conserved pore region of ECaC1/ECaC2 and flanking transmembrane segments.

Cell culture and transfection

Human embryonic kidney cells (HEK293 cell line; gift from Dr David H. MacLennon, University of Toronto, Canada), were grown in Dulbecco's modified Eagle's medium containing 10% (v/v) human serum, 2 mM L-glutamine, 2 U ml^{-1} penicillin and 2 mg ml^{-1} streptomycin at 37°C in a humidity-controlled incubator with 10% CO_2. HEK293 cells were transiently transfected with the pCINeo/IRES-GFP/rbECaC1 or pCINeo/IRES-BFP/mECaC2 vector using methods described previously (Vennekens *et al.* 1999). Transfected cells were visually identified in the patch clamp set up. GFP and BFP were excited at a wavelength between 425 and 475 nm and between 365 and 395 nm, respectively. A 495 nm dichroic mirror was used for GFP and a 420 nm dichroic mirror was used for BFP and finally the emitted light was passed through a 500 nm long-pass filter for GFP and a 430 nm long-pass filter for BFP. The ECaC2-expressing cells were identified by their green or blue fluorescence and GFP- or BFP-negative cells from the same batch were used as controls.

Southern blot analysis

Mice were anaesthetized using 5% v/v isofluran and killed by cervical dislocation in accordance with the guidelines of the Ethical Committee for Animal Experiments of the University of Nijmegen. Subsequently, genomic DNA from tails was prepared by high salt extraction as described previously (Miller *et al.* 1988). Analysis was performed on DNA digested with *Bam*H I and *Eco*R I. DNA was analysed on Southern blots using nylon membranes (Hybond-N, Amersham) hybridized with ^{32}P-labelled (Amersham-USB) mouse ECaC2 probe containing the full, conserved pore-forming region including the flanking transmembrane segments 5 and 6.

Electrophysiology

Electrophysiological methods and Ca^{2+} measurements have been described previously in detail (Vennekens *et al.* 1999). Whole-cell currents were measured with an EPC-9 (HEKA Elektronik, Lambrecht, Germany; sampling rate 0.2 ms, 8-pole Bessel filter 1 kHz) or an L/M-EPC-7 (List Elektronics, Darmstadt, Germany) using ruptured patches. Electrode resistances were between 2 and 5 MΩ, and capacitance values were between 5 and 15 pF. Access resistances varied between approximately 3 and 6 MΩ and were monitored continuously. Series resistance was compensated for approximately 50%. The ramp protocol consisted of linear voltage ramps changing from −100 to +100 mV within 400 ms, applied every 5 s. The step protocol consisted of a series of 60 ms-long voltage steps applied from a holding potential of +20 mV to voltages between +100 and −180 mV with a decrement of 40 mV. To study inactivation and the much slower current decay with Ca^{2+} as the charge carrier, in a single protocol we applied 3 s voltage steps to −100 mV from a holding potential of +70 mV. Fast inactivation was assessed by the time for 10% decay of the current, the slower run down by the time constant of a mono-exponential fit of the current during the last 1.5 s of the step. Current densities, expressed per unit membrane capacitance, were calculated from the current at −80 mV during the ramp protocols.

Solutions and experimental procedures

The standard extracellular solution (Krebs) contained (mM): 150 NaCl, 6 CsCl, 1 $MgCl_2$, 10 Hepes and 10 glucose, pH 7.4 with CsOH, and the concentration of Ca^{2+}, Ba^{2+}, Sr^{2+} or Mn^{2+} was varied between 1 and 30 mM as indicated in the text. Nominally free Ca^{2+} concentration was estimated at 10 μM. Ca^{2+}-free solutions were buffered by 5 mM EGTA at a free [Ca^{2+}] below 1 nM, as calculated by the CaBuf program (G. Droogmans). Monovalent cation currents were inhibited by replacing 150 mM NaCl with an equimolar amount of NMDGCl. The standard internal (pipette) solution contained (mM): 20 CsCl, 100 caesium aspartate, 1 $MgCl_2$, 10 BAPTA, 4 Na_2ATP and 10 Hepes, pH 7.2 with CsOH. To obtain various free Ca^{2+} concentrations in the pipette solution, we added the appropriate amount of Ca^{2+} as calculated with the CaBuf program. In the presence of 10 mM BAPTA, 9.36 mM Ca^{2+} was added to obtain 1 μM free Ca^{2+}, 7.8 mM to obtain 250 nM free Ca^{2+} and 5.8 mM to obtain 100 nM free Ca^{2+}. Cells were kept in a nominally Ca^{2+}-free medium to prevent Ca^{2+} overload and exposed for maximum of 5 min to a Krebs solution containing 1.5 mM Ca^{2+} before sealing the patch pipette to the cell. All experiments were performed at room temperature (20–22°C). In all conditions, control cells (mock-transfected and non-transfected cells) showed only a very small, non-selective current (in the range of 10 pA pF^{-1}) that was blocked by extracellular Ca^{2+} (not shown).

Statistical and phylogenetic analysis

In all experiments, the data are expressed as means ± S.E.M. Overall statistical significance was determined by analysis of variance (ANOVA). In cases of significance ($P < 0.01$), individual groups were compared by Student's t test. Experimental data were fitted to multiple exponentials using the fitting routine of the ASCD program (G. Droogmans). Current traces were fitted to a mono-exponential function using the fitting routine of the WinASCD program (G. Droogmans). Dose–inhibition data were fitted to a dose–response function using Origin software version 6.0 (Microcal Software, Northhampton, MA, USA). The phylogenetic tree was constructed using MegAlign software from Lasergene. The evolutionary tree was calculated by the Clustal method (MegAlign).

RESULTS

Structural and phylogenetic analysis of the ECaC family

Recently, two cDNAs encoding Ca^{2+} channels, ECaC1 and ECaC2, were cloned from rabbit kidney and rat intestine, respectively (Fig. 1*A*). These proteins display a homology of around 75% at the amino acid level and the differences are mainly located at the N- and C-terminal ends. Phylogenetic analysis showed that these Ca^{2+} channels form a separate subfamily among the diverse group of cation channels (Fig. 1*B*). Detailed sequence analysis revealed that these epithelial Ca^{2+} channels contain a unique, conserved pore sequence between transmembrane segments 5 and 6 (Nilius *et al.* 2001*c*). A homologous transcript was recently cloned from rat kidney cortex and named calcium transporter 2 (CaT2; Peng *et al.* 2000*a*). The sequence of rCaT2 is, however, identical to the previously cloned rECaC1 (Hoenderop *et al.* 2000*a*). To investigate whether this ECaC subfamily contains more members besides ECaC1 and ECaC2, Southern blot analysis was performed. Genomic DNA from mice was digested with *Eco*R I or *Xba* I, and hybridized under low stringency with a probe containing the fully conserved pore-forming sequence of ECaC2, including the flanking transmembrane segments. In both digests, only two DNA fragments were detected with this probe and sequence analysis confirmed that these bands correspond to the genes encoding ECaC1 and ECaC2 (Fig. 1*C*).

Tissue distribution of ECaC1 and ECaC2

To investigate in detail the tissue distribution of ECaC1 and ECaC2, various human tissues were evaluated by RT-PCR. With primers specific for ECaC2, a 301 bp

product corresponding to the expected size was amplified in small intestine (duodenum and jejunum), pancreas, placenta, stomach, prostate and testis (Fig. 2). Human ECaC1 was co-expressed with ECaC2 in duodenum, jejunum, placenta, pancreas, prostate and testis. In addition, the ECaC1 transcript was also found in kidney, brain and colon. The nucleotide sequence of the amplified fragments was determined to confirm the specificity of the applied ECaC1 and ECaC2 primer sets.

Currents through ECaC1 and ECaC2; mono- and divalent cation selectivity

Figure 3 shows currents, measured with the whole cell patch-clamp technique, through ECaC1 and ECaC2 heterologously expressed in HEK293 cells. In all experiments, the pipette solution contained 10 mM BAPTA. Figure 3*A*–*D* shows current traces through ECaC1 in response to a voltage step protocol from +60 to −140 mV with 40 mV decrements (holding potential, $V_H = +20$ mV; duration = 60 ms). Extracellular solution contained 150 mM Na^+ and either no divalent cations (Fig. 3*A*), 1 mM Mg^{2+} (Fig. 3*B*), 1 mM Ca^{2+} (Fig. 3*C*) or 30 mM Ca^{2+} (Fig. 3*D*). Figure 3*E* shows current traces in response to a ramp protocol from −100 to +100 mV ($V_H = +20$ mV, duration = 400 ms), in the same ionic conditions as for the voltage steps. ECaC2, like ECaC1, exhibited large non-inactivating currents in the absence of extracellular divalent cations (Fig. 3*A* and *F*). This current was partially blocked in the presence of 1 mM Mg^{2+} (Fig. 3*B* and *G*). Addition of extracellular Ca^{2+} reduced the current amplitude and shifted its reversal potential to significantly more positive potentials, as illustrated in Fig. 3*H* and *I* (see Fig. 3*C* and *D* for comparison with ECaC1). The reversal potential was shifted from -4 ± 1 mV ($n = 13$) in a divalent cation-free solution to 17 ± 2 mV ($n = 6$) and 44 ± 2 mV ($n = 11$), in 1 and 30 mM Ca^{2+}-containing Mg^{2+}-free solution, respectively, consistent with Ca^{2+} permeation through ECaC2 as previously shown for ECaC1 (Vennekens *et al.* 2000). Current inactivation at negative potentials in the presence of 1 or 30 mM Ca^{2+} was obviously faster in ECaC2- than in ECaC1-expressing cells (see below).

The permeation sequence for monovalent cations through ECaC2 as assessed from the current amplitudes at −80 mV was identical to that of ECaC1 (Nilius *et al.* 2000), i.e. $Na^+ > Li^+ > K^+ > Cs^+ \gg NMDG^+$ (Eisenmann X; Fig. 4*A* and *B*). Likewise, the permeation sequence for divalent cations ($Ca^{2+} > Sr^{2+} \approx Ba^{2+} > Mn^{2+}$) was similar to that of ECaC1 (Vennekens *et al.* 2000; Fig. 4*C* and *D*). Notably, the ratio between the amplitude of the currents carried by Ba^{2+} and Ca^{2+}, I_{Ba}/I_{Ca}, was significantly higher for ECaC1 than for ECaC2, i.e. 0.69 ± 0.05 ($n = 12$) compared to 0.39 ± 0.03 ($n = 15$), indicating that ECaC1 is more permeable to Ba^{2+} compared with ECaC2.

Anomalous mole fraction behaviour between Ca^{2+} and Na^+ and block by Mg^{2+} and ruthenium red

As previously described for ECaC1 (Vennekens *et al.* 2001*a*) and other Ca^{2+}-selective channels (Almers & McCleskey, 1984; Hess *et al.* 1986; Lepple-Wienhues & Cahalan, 1996), we were able to show an anomalous mole fraction behaviour for ECaC2 in the presence of Ca^{2+} and Na^+. Figure 5*A* shows currents in response to a ramp protocol from −100 to +100 mV in the absence of extracellular Mg^{2+} and in the presence of 150 mM Na^+, at extracellular Ca^{2+} concentrations ($[Ca^{2+}]_o$) ranging from 10 nM to 30 mM. Figure 5*B* (filled squares) shows the pooled data of the corresponding current amplitudes at −80 mV normalized to that in EGTA-buffered divalent cation-free solution. Increasing $[Ca^{2+}]_o$ up to 100 μM reduced the current, but a further increase to 30 mM enlarged the current again. Apparently, Ca^{2+} blocks monovalent cation currents through ECaC2 with an IC_{50} of about 150 nM, which is comparable to the value obtained for ECaC1 (200 nM; Vennekens *et al.* 2001*a*).

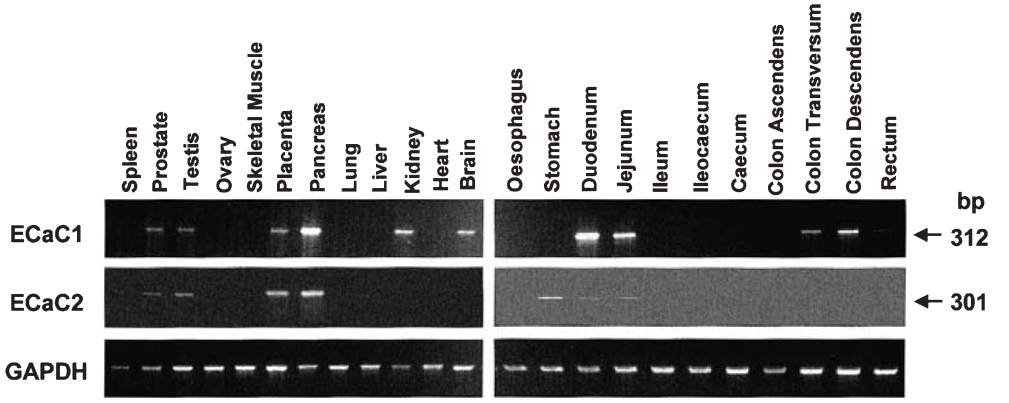

Figure 2. Tissue distribution of the ECaC family

Distribution of human ECaC1 and ECaC2 mRNA in a panel of human tissue-derived cDNAs. Expected length of the PCR fragments for ECaC1 (312 bp) and ECaC2 (301 bp) is indicated. The amplified GAPDH fragment demonstrates the integrity of the cDNA samples.

Table 1. Two-binding site permeation model

	Outer barrier		Well (binding site)		Central barrier		
	Na^+	Ca^{2+}	Na^+	Ca^{2+}	Na^+	Ca^{2+}	Q
ECaC2	9	10	−0.7	−16.5	22.6	−6.5	3.5
ECaC1	10	10.5	−1	−16.7	−22.6	−6.5	17.7
Hess & Tsien (1984)	4.5	10	−15	1	−6	8	3
Almers & McCleskey (1984)	10.3	10	−14.5	−2	0	10	11.89

Summary of the parameters (in RT units) used for a two-binding site permeation model for ECaC1 and 2. For comparison, parameters are shown for the two-binding site model for the L-type Ca^{2+} channel pore (Hess & Tsien, 1984; Almers & McCleskey, 1984).

It is possible to fit this anomalous mole fraction behaviour to a mathematical pore model; e.g. a two-binding site model of which the classical example is the model developed for L-type voltage-activated Ca^{2+} channels (Hess & Tsien, 1984; Almers & McCleskey, 1984; Vennekens *et al.* 2001*b*). In this model, the channel pore contains two high-affinity binding sites. An energy profile of the channel pore can be calculated, which is assumed to be symmetrical with equidistant barrier and wells. The wells are energy minima representing binding sites and the peaks are electrochemical barriers the ion has to overcome to go from one binding site to the other or

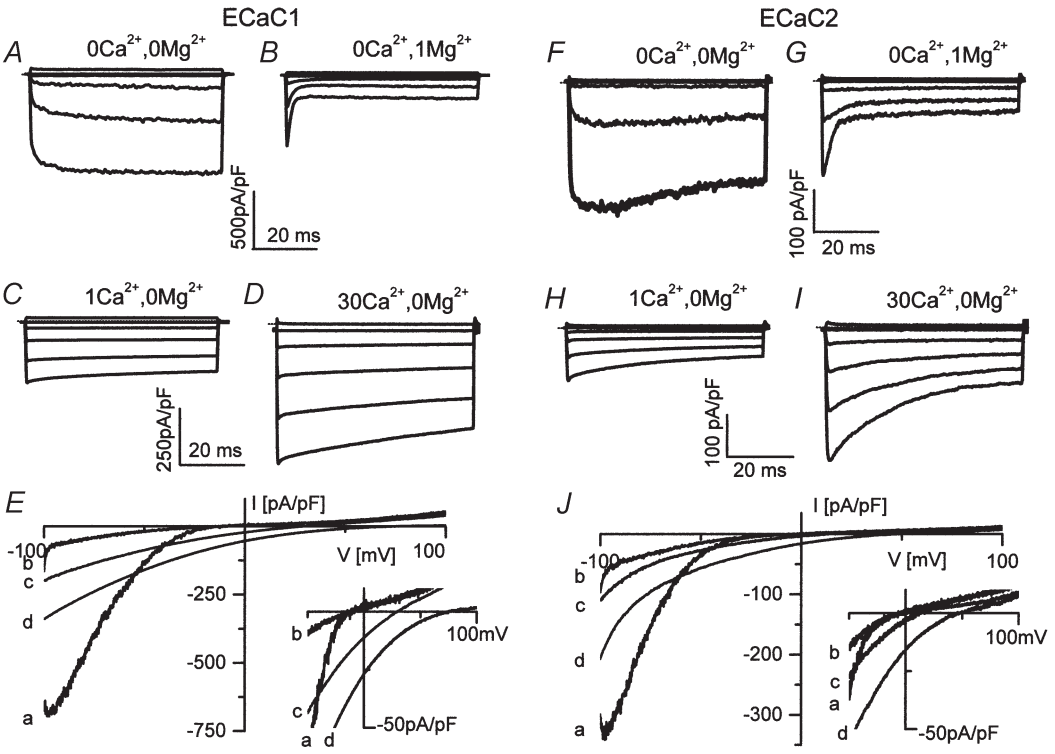

Figure 3. Currents through ECaC1 and ECaC2

A–D, currents in response to a voltage step protocol from +60 to −140 mV with 40 mV decrements (V_H = +20 mV and duration = 60 ms), recorded from an ECaC1-expressing HEK293 cell. Extracellular Ca^{2+} and Mg^{2+} (mM) were applied as indicated. $[Ca^{2+}]_i$ was buffered with 10 mM BAPTA through the pipette solution in all experiments. *E* and *J*, current traces in response to a 400 ms ramp from −100 to +100 mV from a holding potential of +20 mV, recorded from an ECaC1- or ECaC2-expressing HEK293 cell in an extracellular solution with 0 mM Ca^{2+}, 0 mM Mg^{2+} (a); 0 mM Ca^{2+}, 1 mM Mg^{2+} (b); 1 mM Ca^{2+}, 0 mM Mg^{2+} (c); and 30 mM Ca^{2+}, 0 mM Mg^{2+} (d). The *y*-axis scale is expanded in the insets to show the reversal potential of the currents more clearly. *F–I*, currents in response to voltage steps ranging from +60 to −140 mV with 40 mV decrements (V_H = +20 mV and duration = 60 ms), recorded from an ECaC2-expressing HEK293 cell. Extracellular Ca^{2+} and Mg^{2+} (mM) were applied as indicated. Intracellular Ca^{2+} was buffered in all experiments with 10 mM BAPTA added to the pipette solution.

to enter or leave the pore (Hess & Tsien, 1984; Almers & McCleskey 1984; see inset of Fig. 5*B*).

The continuous line in Fig. 5*B* represents the fit that was generated with this model for ECaC2, using the energy profile depicted in the inset. The heights of the outer energy barriers, i.e. 10 and 9 *RT* units (in which *R* is the gas constant and *T* is the absolute temperature) for Ca^{2+} and Na^{+}, respectively, are in the range expected for diffusional access to and departure of ions from the pore. Other parameter values are summarized in Table 1. In low Ca^{2+} concentrations, no Ca^{2+} ions are bound to the high-affinity Ca^{2+}-binding sites and the channel pore is freely permeable for monovalent ions. When the Ca^{2+} rises to micromolar concentrations, a single Ca^{2+} ion will be bound to one of the binding sites and will block monovalent cation currents through the channel. The IC_{50} for the blocking of monovalent cation currents by Ca^{2+} can be used to estimate the depth of the energy well for both binding sites, i.e. −16.5 corresponding to a dissociation constant of 150 nM. When $[Ca^{2+}]_o$ rises further, both binding sites will be occupied by $[Ca^{2+}]_o$ ions and the mutual repulsion between the two ions will deliver the driving force of Ca^{2+} permeation through the channel. This is accounted for by the repulsion factor *Q*, which affects both the on and off rate of Ca^{2+} ions binding to the binding sites (for a more thorough discussion of the model see Hess & Tsien, 1984; Almers & McCleskey, 1984). The dotted line in Fig. 5*B* represents the fit that was generated for the data of ECaC1 (Vennekens *et al.* 2001*a*). Table 1 summarizes the parameters used for ECaC1, ECaC2 and the L-type voltage-activated Ca^{2+} channel. The main difference between the ECaCs lies in the repulsion factor *Q*, which provides the drive for ionic permeation through the channel. Concomitantly, it is shown in Fig. 5*B* that the reduction of the current through ECaC2 at sub-micromolar Ca^{2+} concentrations is more pronounced than in ECaC1, and the increase of the current through ECaC2 at Ca^{2+} concentrations above 1 μM is not as great as that through ECaC1. This difference in permeation between the channels is, therefore, most probably due to specific pore properties of these channels.

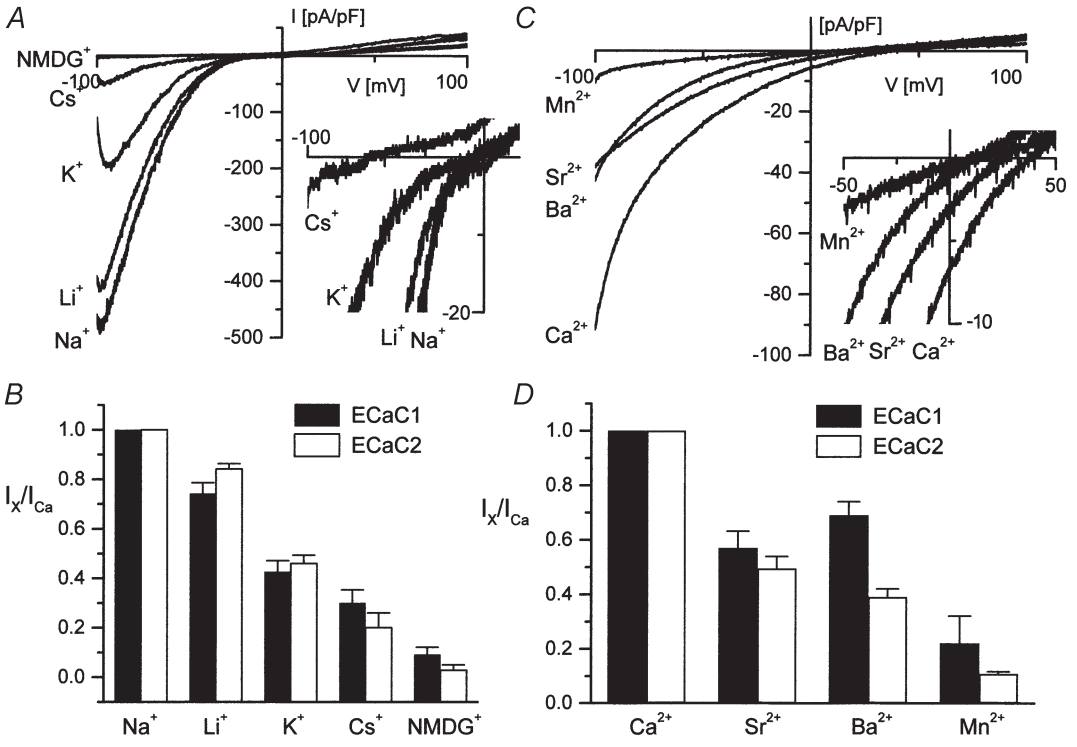

Figure 4. Mono- and divalent cation permeation through ECaC1 and ECaC2

A, current traces for ECaC2 in response to a ramp protocol as in Fig. 3, in divalent cation-free extracellular solutions containing 150 mM Na^{+}, 150 mM Li^{+}, 150 mM K^{+}, 150 mM Cs^{+} or 150 mM $NMDG^{+}$. The *y*-axis scale is expanded in the inset to show the reversal potential of the currents more clearly. *B*, normalized current values measured at −80 mV from linear voltage ramps as above. Currents were normalized to the current value in 150 mM Na^{+} solution. Number of cells: six for ECaC1 and five for ECaC2. *C*, current traces for ECaC2 in response to a ramp protocol as in Fig. 3, in solutions containing 30 mM Ca^{2+}, 30 mM Ba^{2+}, 30 mM Sr^{2+} or 30 mM Mn^{2+}. The *y*-axis scale is expanded in the inset to show the reversal potential of the currents more clearly. *D*, normalized current values measured at −80 mV from linear ramps as described above. Currents were normalized to the current value in the 30 mM Ca^{2+} solution. Number of cells: eight for ECaC1 and three for ECaC2.

As shown in Fig. 1*A*, a single aspartic acid residue is conserved at position 547 in the pore region of mouse and rat ECaC2, whereas the rabbit and rat ECaC1 transcripts contain a serine residue at the corresponding position (residue 548). To investigate whether this extra negative charge is responsible for the altered properties of ECaC2 compared to ECaC1, we mutated this aspartic acid residue to a serine in ECaC2 (D547S) and, *vice versa*, the serine residue to an aspartic acid in ECaC1 (S548D). In neither of these constructs were the respective wild-type properties affected (not shown). The current in the presence of 100 μM extracellular Ca^{2+} normalized to that in Ca^{2+}-free solution was 0.09 ± 0.02 ($n = 10$) for wild-type ECaC1 compared to 0.09 ± 0.02 ($n = 8$) for the mutant channel (S548D). For wild-type ECaC2 we found a value of 0.03 ± 0.01 ($n = 5$) compared to 0.020 ± 0.003 ($n = 7$) for the mutant channel (D547S). Furthermore, we studied the affinity of ECaC2 for extracellular Mg^{2+} (Fig. 6*A*). The estimated IC_{50} values were 200 ± 14 μM ($n = 14$) in Ca^{2+}-free solution, 1.4 ± 0.2 mM ($n = 10$) in the

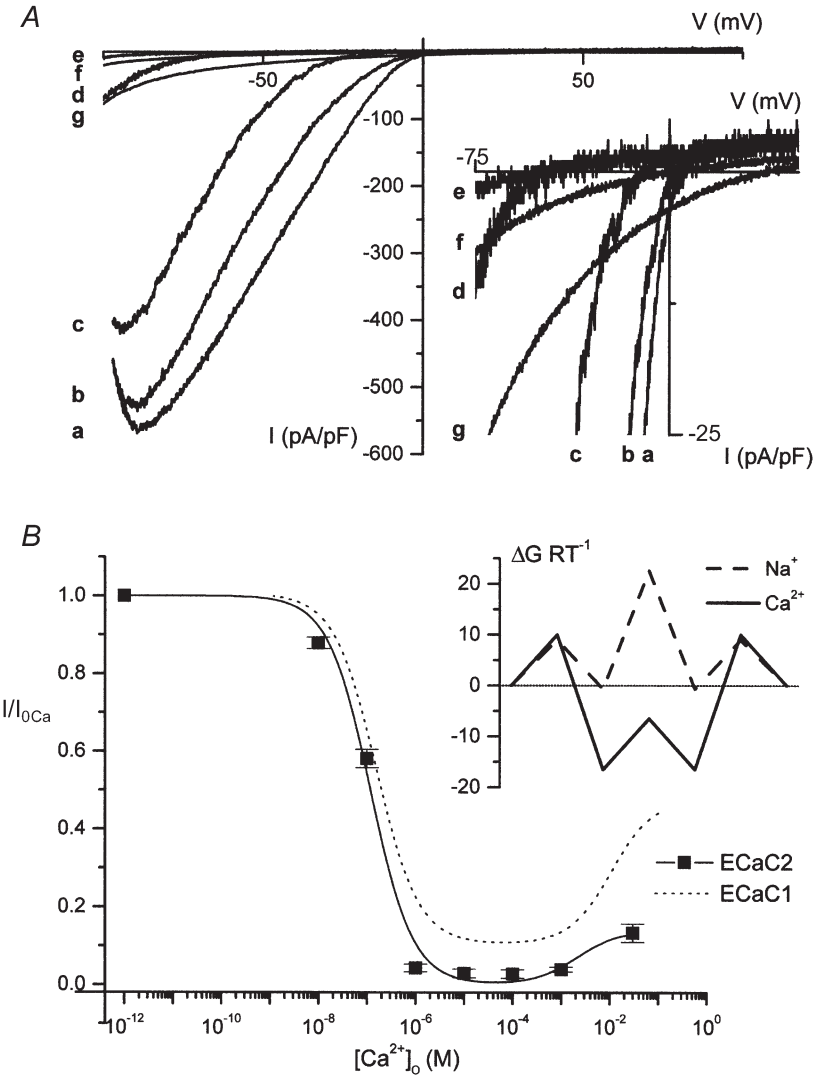

Figure 5. Anomalous mole fraction behaviour of ECaC2

A, currents through ECaC2 in response to a voltage ramp from −100 to +100 ($V_H = +20$ mV, duration = 400 ms). Cells were loaded with 10 mM BAPTA. Various extracellular Ca^{2+} concentrations were applied, in the absence of extracellular Mg^{2+}: Ca^{2+}-free EGTA-buffered solution (a); 10 nM Ca^{2+} (b); 100 nM Ca^{2+} (c); 1 μM Ca^{2+} (d); 100 μM Ca^{2+} (e); 1 mM Ca^{2+} (f); 30 mM Ca^{2+} (g). The *y*-axis scale is expanded in the inset to show the reversal potential of the currents more clearly. *B*, mean normalized current values measured at −80 mV during linear voltage ramps in various $[Ca^{2+}]_o$. Currents were normalized to the current value from the same cell in Ca^{2+}-free solution. ■, data points for ECaC2. The continuous line represents the fit as generated by the two-binding site model for ECaC2 (see Results for details). The dotted line represents the fit for ECaC1. Fit parameters are summarized in Table 1. The inset shows the energy profiles of the ECaC2 pore along the path of the pore for Ca^{2+} and Na^+ (in RT values; for details see Results).

presence of 100 μM extracellular Ca^{2+} and up to 9 mM in the presence of 1 mM extracellular Ca^{2+}. These values are of the same order of magnitude as those described previously for ECaC1 (see Vennekens *et al.* 2001*a*); IC_{50} values were 62 ± 9 μM ($n = 4$) and 328 ± 50 μM ($n = 4$–9) in the absence of extracellular Ca^{2+} and in the presence of 100 μM Ca^{2+}, respectively. In the presence of 1 mM Ca^{2+} this value shifted up to 5 mM. Also, we investigated the affinity of ECaC2 for ruthenium red. This compound blocks ECaC1 with an IC_{50} of 121 ± 13 nM ($n = 5$–9; Nilius *et al.* 2001*b*). ECaC2, on the other hand, was blocked with an IC_{50} value of 9 ± 1 μM ($n = 5$; Fig. 6*B*). The mutations in the pore region described above, ECaC1 (S547D) and ECaC2 (D548S), had no effect on these IC_{50} values indicating that these residues are not involved in the binding of ruthenium red to the channel (not shown).

Ca^{2+}-dependent decay and inactivation of Ca^{2+} currents through ECaC1 and ECaC2

The decay of Ca^{2+} currents through ECaC1 during successive ramps and its inactivation at negative potentials in the presence of extracellular Ca^{2+}, which are both largely abolished when Ba^{2+} is the charge carrier, represent the most characteristic features of the channel (Vennekens *et al.* 2000). However, during a successive ramp protocol, the cell membrane is mostly at a depolarized holding potential (+20 mV in our case), allowing channels to recover from inactivation. Therefore, to probe the inactivation process over a continuous period of time we used a long step protocol consisting of 3 s steps to −100 mV from a holding potential of +70 mV (Fig. 7*A* and *B*). It is clear that inactivation in response to such a voltage step is a Ca^{2+}-dependent process. When 30 mM Ba^{2+} was used as the charge carrier the percentage inactivation after 3 s was significantly smaller in the case of both ECaC1 and ECaC2. On the other hand, the percentage inactivation after 3 s did not differ significantly between the channels when either Ca^{2+} or Ba^{2+} was used as the charge carrier. Inactivation during the voltage step protocol is a multi-phasic process. The initial phase of the current decline, as illustrated at higher time resolution in Fig. 3, is much faster in ECaC2-expressing cells than in ECaC1-expressing cells, and is followed by a slower phase. To

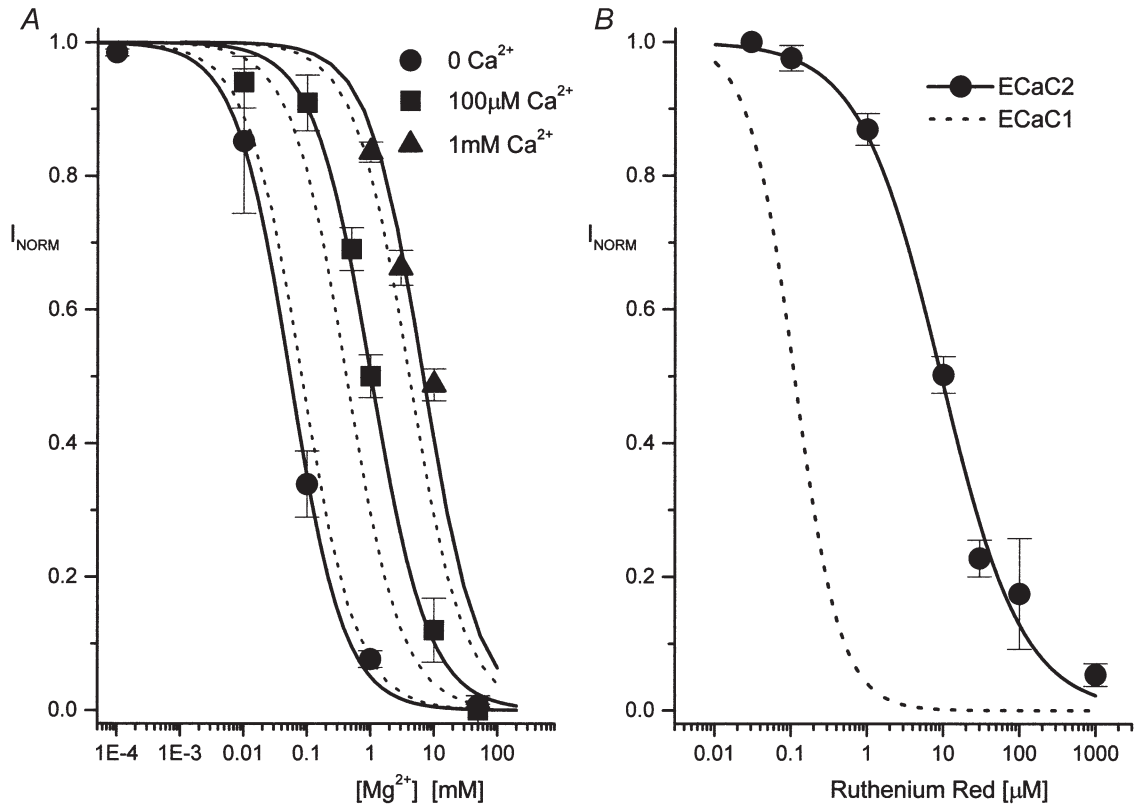

Figure 6. Dose–inhibition analysis for extracellular Mg^{2+} and ruthenium red on ECaC1 and ECaC2

A, pooled data for the inhibition of currents through ECaC1 and 2 in the presence of three different Ca^{2+} concentrations. Data were gathered from linear voltage ramps (as above) at −80 mV. Filled symbols and continuous lines represent data points and the logistic fit for ECaC2, respectively. Dashed lines represent the logistic fit for ECaC1. *B*, pooled data for the inhibition of monovalent cation currents through ECaC1 and 2 by ruthenium red. Data were gathered from linear voltage ramps (as above) at −80 mV. Filled symbols and the continuous line represent data points and the logistic fit for ECaC2, respectively. The dashed line represents the logistic fit for ECaC1.

discriminate between the two components, we used the time to 10 % current reduction ($t_{10\%}$) as a measure of fast inactivation and the time constant of the exponential fitted to the current during the last 1.5 s of the current trace ($\tau_{1.5\,s}$) to assess the slow component of current decay. The $t_{10\%}$ value of 19 ± 4 ms ($n = 9$) for Ca^{2+} currents through ECaC2 was significantly shorter than the value for Ba^{2+} currents, i.e. 903 ± 112 ms ($n = 10$; Fig. 7*D*). A similar Ca^{2+} dependence for the fast inactivating component was found for ECaC1, i.e. 167 ± 33 ms ($n = 8$) for Ba^{2+} currents compared to 69 ± 12 ms ($n = 8$) for Ca^{2+} currents. Strikingly, the $t_{10\%}$ value for Ca^{2+} currents was significantly different between ECaC1 and ECaC2, i.e. 69 ± 12 ms ($n = 8$) and 19 ± 4 ms ($n = 9$), respectively. The $\tau_{1.5\,s}$ values of the slow component of 481 ± 45 ms ($n = 9$) for ECaC1 and 513 ± 35 ms ($n = 21$) for ECaC2 were not significantly different (not shown). It is important to note here that the percentage inactivation of currents in our voltage step protocol depended on the size of the peak current. At high current densities (up to 1 nA pF^{-1}) that can be obtained in our expression system, there was no significant difference between the percentage inactivation after 3 s when either Ca^{2+} or Ba^{2+} was the charge carrier. This points to a mechanism for the slowly inactivating current phase for ECaC1 and ECaC2 that does not depend on Ca^{2+} as the charge carrier at these high current densities (data not shown). Therefore, we restricted the current densities in the above analysis to 250 pA pF^{-1}.

Previously, we have analysed the modulation of ECaC1 by intracellular Ca^{2+} (Nilius *et al.* 2001*a*). Increasing $[Ca^{2+}]_i$ by dialysing cells with various concentrations revealed an inhibition of monovalent cation currents through ECaC1 with an estimated IC_{50} value of 82 nM ($n = 6$–8). Applying the same protocol to ECaC2-expressing cells, we found that $[Ca^{2+}]_i$ blocks monovalent cation currents through this channel with an IC_{50} value of about 129 nM ($n = 6$), which is of the same order of magnitude as for ECaC1 (Fig. 7*E*). In the presence of

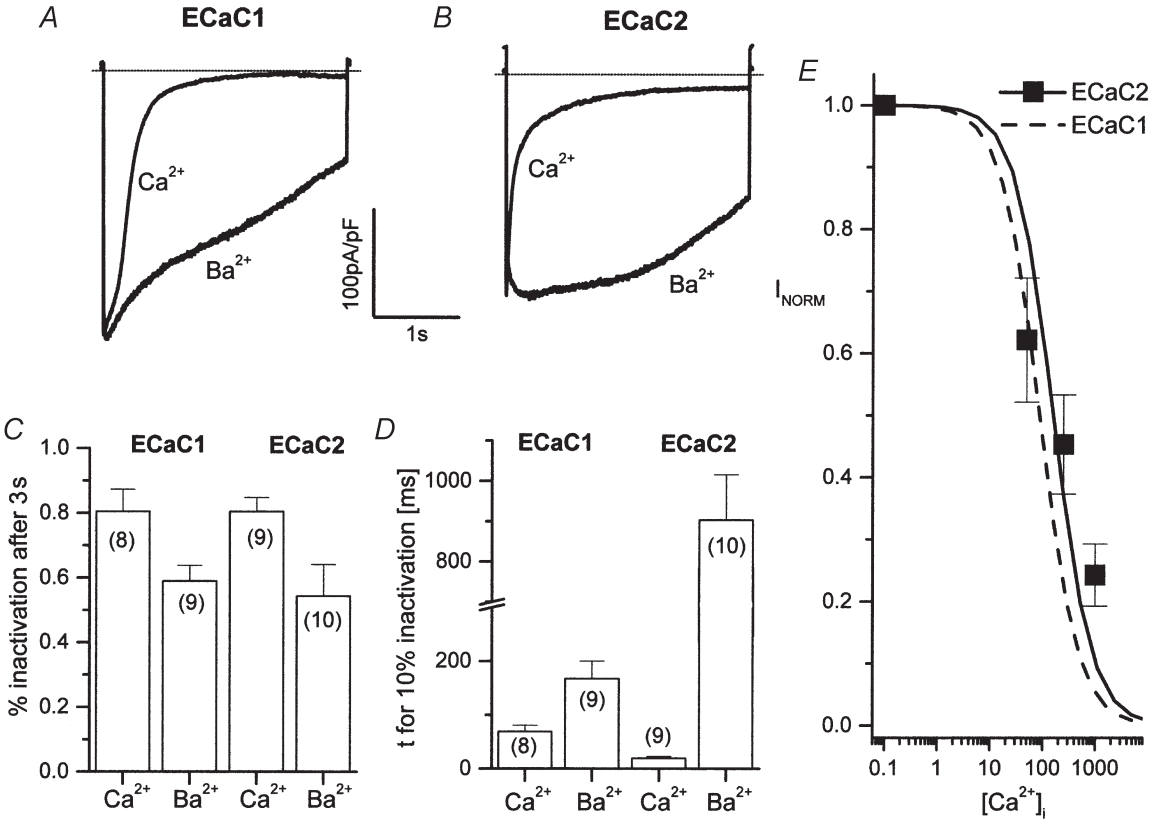

Figure 7. Inactivation of ECaC1 and ECaC2 currents in 30 mM $[Ca^{2+}]_o$

A–*B*, currents through ECaC1 and ECaC2 in response to a voltage step to −100 mV ($V_H = +70$ mV) in the presence of 30 mM $[Ca^{2+}]_o$ or $[Ba^{2+}]_o$ and 150 mM $NMDG^+$ as indicated. Cells were loaded with 10 mM BAPTA. *C*, pooled data comparing the ratio between the peak current and the current at the end of the 3 s voltage step with either Ca^{2+} or Ba^{2+} as the charge carrier, in the case of ECaC1 and ECaC2; *n* values are indicated in parentheses. *D*, pooled data comparing the time for 10 % inactivation ($t_{10\%}$) during a voltage step, as in *A* and *B*, between ECaC1 and ECaC2; *n* values are indicated in parentheses. *E*, dose–inhibition analysis for the inhibition of monovalent cation currents through ECaC channels by intracellular Ca^{2+} in the absence of extracellular divalent cations ($n = 6$–8). Data points were normalized to the current density in 10 nM $[Ca^{2+}]_i$, i.e. 2143 ± 159 pA pF^{-1} ($n = 8$).

1 mM $[Ca^{2+}]_o$ and $NMDG^+$ in place of extracellular Na^+, the IC_{50} for ECaC1 inhibition shifted to 89 nM in comparison with 74 nM in the case of ECaC2.

Another interesting aspect of Ca^{2+}-dependent regulation is the recovery of ECaCs from inactivation. In this study, we compared cells that showed a similar amount of inactivation after a 3 s voltage step in the presence of 30 mM Ca^{2+}. Recovery was probed subsequent to an inactivating step by successive ramps in the absence of extracellular divalent cations, and current densities were compared to the current value in divalent cation-free conditions before the application of the voltage protocol. ECaC1 and ECaC2 recovered completely from inactivation within 5–7 min. On average, after 5 min currents through ECaC2 had recovered to 94 ± 3 % ($n = 9$) of the value before the inactivating step; currents through ECaC1 had recovered to 95 ± 2 % ($n = 15$) of the value before inactivation. It is clear from our data that recovery from inactivation is a Ca^{2+}-dependent process (Fig. 8*A* and *B*) as assessed by the half-time ($t_{½}$) of recovery from inactivation. For ECaC1, $t_{½}$ for recovery was 83 ± 12 s ($n = 17$) after inactivation in the presence of 30 mM Ca^{2+} compared to 7 ± 3 s ($n = 6$) in the presence of Ba^{2+}. Moreover, recovery from Ca^{2+}-dependent inactivation was significantly faster in the case of ECaC2, i.e. $t_{½}$ was 33 ± 7 s ($n = 8$) for ECaC2 compared to 83 ± 12 s ($n = 17$) for ECaC1 (Fig. 8*C* and *D*).

Dependence of ECaC1 and ECaC2 on intracellular ATP and Mg^{2+}

We tested whether ECaC1 and ECaC2 are dependent on intracellular ATP and Mg^{2+} concentrations. As can be seen from the time course of an experiment (currents normalized to peak current density) at −80 mV (Fig. 9*A*), monovalent cation currents through ECaC1 showed

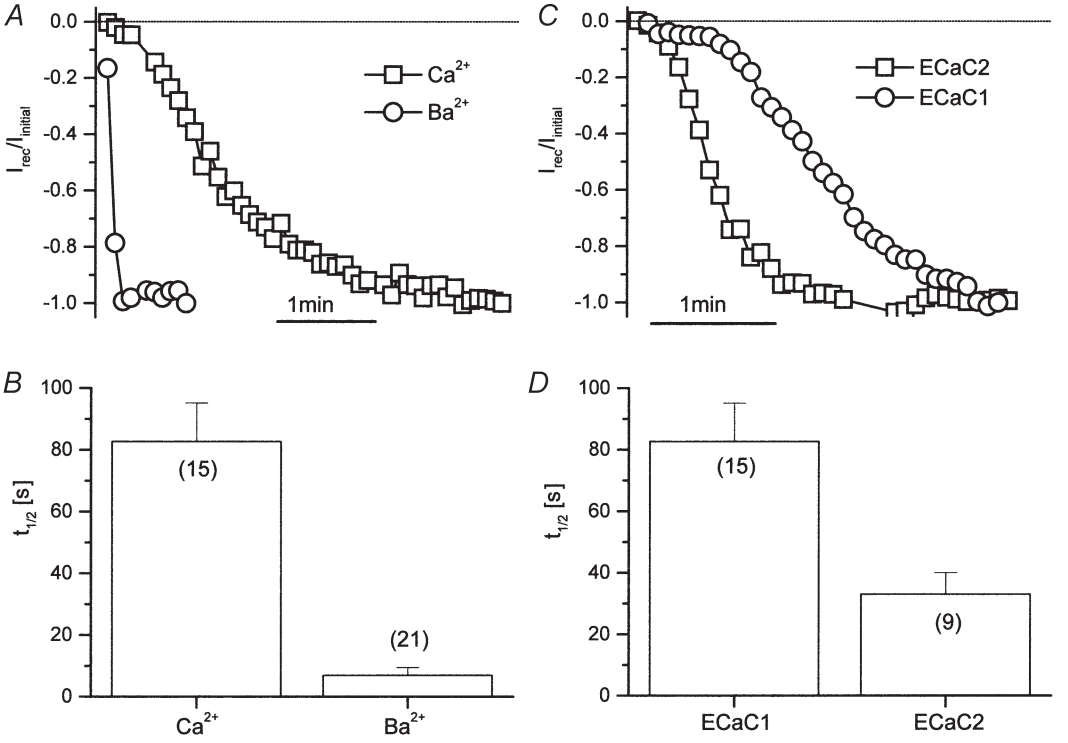

Figure 8. Recovery from inactivation for ECaC1 and ECaC2

A, time course of the recovery from inactivation at −80 mV for ECaC1. I_{rec}/I_{init} represents the ratio between the current amplitude before the inactivating step and the current amplitude after the inactivating step as a function of time. Cells were subjected to an inactivating step as in Fig. 7. Time course is shown for the case when Ca^{2+} or Ba^{2+} was the charge carrier during the inactivating step. Subsequently external solution was changed to divalent cation-free solution and linear voltage ramps (as above) were applied, each 5 s. *B*, pooled data for the half-time of recovery from inactivation of ECaC1 when either Ca^{2+} or Ba^{2+} was the charge carrier during the inactivating step; *n* values are indicated in parentheses. *C*, time course of the recovery from inactivation at −80 mV for ECaC1 and ECaC2. Cells were subjected to an inactivating step as in Fig. 7 in the presence of 30 mM $[Ca^{2+}]_o$. Subsequently, external solution was changed to divalent cation-free solution and linear voltage ramps (as above) were applied each 5 s. *D*, pooled data comparing the half-time for recovery from inactivation when Ca^{2+} was the charge carrier during the inactivating step, in the case of ECaC1 and ECaC2; *n* values are indicated in parentheses.

almost no decay in the presence of (nominally) 1 mM Mg^{2+} and 4 mM ATP intracellularly. In the absence of intracellular ATP, however, currents showed a fast decay, which was only partly abolished when Mg^{2+} was also removed from the intracellular solution. In the presence of 10 mM Mg^{2+} and 0 mM ATP decay of the currents was extremely fast, indicating that intracellular Mg^{2+} was indeed blocking ECaC1. Furthermore, it is clear that intracellular ATP was also necessary to maintain stable channel activity. In the case of ECaC2, it was even more dramatic (Fig. 9*B*). While in the presence of 1 mM $[Mg^{2+}]_i$ and 4 mM $[ATP]_i$ monovalent cation currents through ECaC2 were highly stable, they dramatically decayed in the absence of both ATP and Mg^{2+}. This decay was aggravated with increasing Mg^{2+} concentrations.

DISCUSSION

The expression cloning of epithelial Ca^{2+} channels from rabbit kidney (ECaC1) and rat intestine (ECaC2) has provided a molecular basis to study the process of Ca^{2+} entry in Ca^{2+}-transporting epithelia. A complete understanding of the structural and functional relationship between these two related proteins requires extensive characterization using identical experimental conditions, as we described in the present study.

Phylogenetic analysis demonstrated that ECaC1 forms a subfamily of Ca^{2+} channels, which can be placed together with the vanilloid receptors in the OTRPC channel group (Harteneck *et al.* 2000). Previous electrophysiological studies performed with HEK293 cells heterologously expressing ECaC1 demonstrated functional characteristics of ECaC1 that are unique to this Ca^{2+}-permeable cation channel family (Nilius *et al.* 2001*c*). ECaC1 contains a distinguishing pore sequence that is clearly different from the vanilloid receptors and members of the TRP family, and this could explain the high selectivity for Ca^{2+} (Nilius *et al.* 2001*c*). The fully conserved pore sequence of ECaC1 and 2 has been used to identify additional members of the ECaC family. Southern blot analysis demonstrated that this pore sequence is restricted to the previously identified genes encoding ECaC1 and ECaC2, suggesting that the ECaC family is limited to these two members, which originate from two independent genes juxtaposed on chromosome 7q35 (Müller *et al.* 2000*b*). Confusingly, Peng *et al.* (2000*a*) recently identified a transcript from rat kidney cortex, named calcium transporter 2 or CaT2, which only differs by four amino acids from the previously cloned rECaC. Together with our Southern blot analysis, this indicates that the ECaC1 gene encodes CaT2. Minor variation between these two transcripts could be explained by

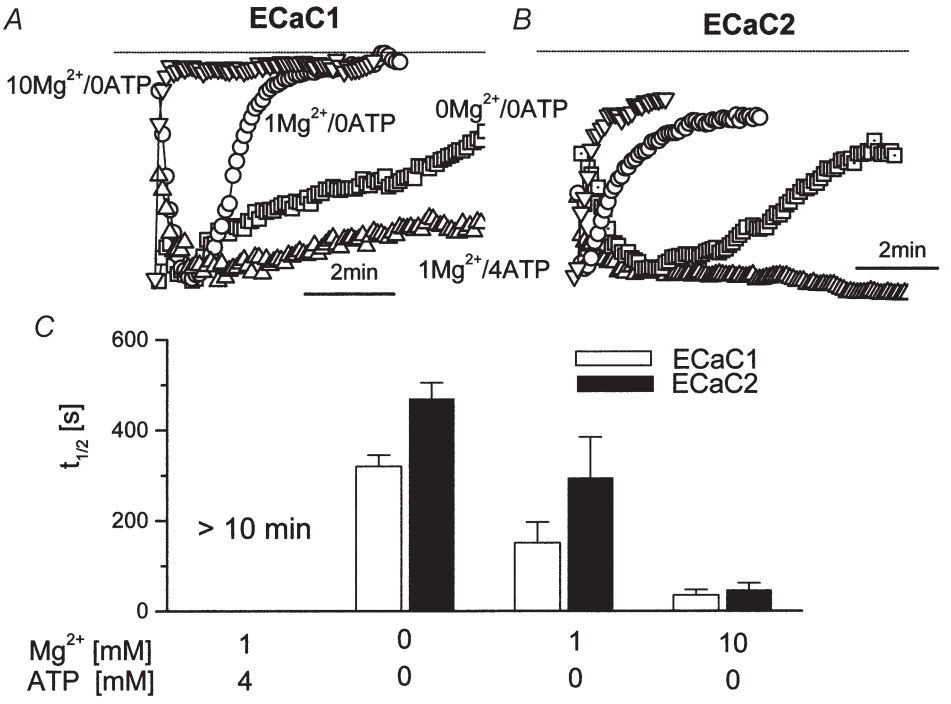

Figure 9. Sensitivity of ECaC1 and ECaC2 to intracellular Mg^{2+} and ATP

A–B, time course of normalized monovalent cation currents through ECaC1 and ECaC2 in the presence of various intracellular Mg^{2+} and ATP concentrations as indicated. Data points were recorded at −80 mV from linear voltage ramps (as above) and normalized to the peak current value. The first point of the data line represents the start of the whole-cell measurement after breaking through the membrane patch. *C*, pooled data comparing the half-time for decay of monovalent cation currents through ECaC channels, with various intracellular ATP and Mg^{2+} concentrations as indicated ($n = 3–6$ for each data point).

different rat strains or nucleotide polymorphisms. To avoid further confusion in nomenclature of the ECaC family, we would prefer to use the abbreviations ECaC1 and ECaC2 instead of CaT2 and CaT1, respectively. The Human Gene Mapping Workshop-approved symbol of the corresponding human genes is indeed ECAC1 (Müller *et al.* 2000*b*) and ECAC2 (Barley *et al.* 2001). Furthermore, the two proteins have been shown to function as Ca^{2+}-selective ion channels rather than as transporters (Vennekens *et al.* 2000; present study).

RT-PCR analysis on various human tissues using specific primer sets for ECaC1 and ECaC2 revealed expression of ECaC2 in the small intestine (duodenum and jejunum), placenta, pancreas, stomach, testis and prostate. A similar expression profile was observed for ECaC1 with the exception of stomach (Müller *et al.* 2000*a*). In addition, the ECaC1-positive tissues also expressed the calcium-binding protein calbindin D (Müller *et al.* 2000*a*) and the present study extends this observation for ECaC2-containing tissues, with the exception of stomach, which does not contain one of the calbindins. Interesting in this respect is the previous finding that Ca^{2+} absorption occurs in rumen, but further studies are required to investigate the function of ECaC2 in this organ (Wadhwa & Care, 2000). In addition, expression of ECaC1, unlike ECaC2, was found in colon and kidney. Together with the expression in duodenum, jejunum, rectum and the absence in ileum and caecum this segmental distribution corresponds to the occurrence of 1,25-dihydroxyvitamin D_3-regulated Ca^{2+} (re)absorption in humans (Elsharyday *et al.* 1995). Recently, a similar distribution was observed for human ECaC2 by Northern blot analysis (Peng *et al.* 2000*b*).

In the past, species differences have been observed for the process of Ca^{2+} absorption in the intestinal tract and the present study suggests that this is also reflected in the expression profile of ECaCs. For instance, ECaC1 could be easily detected in human colon, whereas rabbit colon does not express this transcript (Hoenderop *et al.* 1999*a*). This is in line with the observed differences in the process of Ca^{2+} absorption between these two species. In humans, ECaC2 expression was not observed in caecum (this study), whereas Peng *et al.* (1999) described a high expression in rat caecum. It has been demonstrated, however, that the caecum is the site with the highest calcium absorption in the rat intestine, whereas in humans this process primarily occurs in the duodenum (Karbach & Feldmeier, 1993).

We performed whole-cell patch-clamp measurements of Ca^{2+} currents through ECaC2 heterologously expressed in HEK293 cells, and compared its electrophysiological properties with those of ECaC1. As may be expected from the highly conserved pore sequence of the two channels, ECaC2 permeation properties were comparable to those of ECaC1. ECaC2 showed an anomalous mole fraction behaviour between Ca^{2+} and Na^+, as was described for ECaC1 (Hess *et al.* 1986; Vennekens *et al.* 2000). A peculiar difference in this regard is the smaller increase of the ECaC2 currents compared to ECaC1 currents at elevated $[Ca^{2+}]_o$. It is possible to describe this anomalous mole fraction effect for ECaC1 by assuming a pore structure with two high-affinity Ca^{2+}-binding sites, as described for L-type voltage-gated Ca^{2+} channels (Hess & Tsien, 1984; Vennekens *et al.* 2001*b*). Thus, these differences most probably reflect slight differences of the permeation mechanism between ECaC1 and ECaC2. Interestingly, alignment of the pore region of ECaC1 and ECaC2 revealed the presence of an additional negative charge (i.e. an aspartate residue, D547) in the ECaC2 pore, which is conserved in mouse and rat ECaC2, whereas ECaC1 has a serine residue (S548) at the corresponding position. However, mutating the serine residue in ECaC1 to an aspartate (S548D) and, *vice versa*, changing the aspartate residue in ECaC2 to a serine (D547S) had no effect on the normalized current values in micro- and millimolar Ca^{2+} concentrations. It is, therefore, unlikely that this amino acid could account for the different pore properties of ECaC1 and ECaC2. Furthermore, the permeability sequence for the monovalent and divalent cation current is almost identical in the two channels. However, the relative permeability for Ba^{2+} in relation to Ca^{2+} was significantly smaller for ECaC2 compared to ECaC1. The affinity of ECaC2 for Ca^{2+} and Mg^{2+}, as measured by the concentration for half-maximal inhibition of the monovalent cation current, is of the same order of magnitude as for ECaC1. Importantly, however, for the first time a pharmacological distinction can be made between ECaC1 and ECaC2 with ruthenium red, for which ECaC2 has a 100-fold lower affinity compared to ECaC1.

Slight differences were found in the Ca^{2+}-dependent feedback mechanism, which is reflected in the Ca^{2+}-dependent inactivation of currents in response to a hyperpolarizing voltage step. We show here that Ca^{2+} currents through ECaC2 exhibit somewhat different inactivation kinetics compared to ECaC1, although the total amount of inactivation was not significantly different between the channels. On the other hand, we could demonstrate that ECaC2 recovered twice as fast from inactivation compared to ECaC1, indicating that the main difference between the channels will presumably lie in the recovery mechanism, rather than the inactivation mechanism itself.

We show here for the first time the modulation of ECaCs by intracellular Mg^{2+} and ATP. It is clear from our data that the activity of ECaC1 and ECaC2 rapidly decays in the absence of intracellular ATP and this effect is further accelerated at higher intracellular Mg^{2+} concentrations. Recently it was shown that another member of the TRP family, LTRPC7, is modulated by intracellular Mg^{2+}-ATP (Nadler *et al.* 2001). It will be interesting to explore common molecular determinants between LTRPC7 and ECaCs for the mechanism of this modulation.

Recently, two papers have presented electrophysiological data on ECaC2 (Suzuki *et al.* 2000; Yue *et al.* 2001). In the latter study, ECaC2 was expressed in CHO cells and displayed the same properties as described here, at least concerning divalent cation selectivity and increased monovalent cation permeability in the absence of extracellular divalent cations. Strikingly, however, the authors describe an IC_{50} value for block of monovalent cation currents by extracellular Ca^{2+} of about 3 μM, i.e. 30 times higher than the value obtained in the present study. Furthermore, ECaC2 has been postulated to function as a store-operated channel when expressed in CHO cells. In a second paper, Suzuki *et al.* (2000) have also expressed ECaC1 and ECaC2 in CHO cells. However, the overall view of the reported currents is highly contrasting with the results that we have gathered. It is unlikely that this is due to the differential expression system since Yue *et al.* (2001) also used CHO cells.

In summary, the epithelial Ca^{2+} channel family is a unique group of Ca^{2+}-selective channels consisting of only two highly homologous members, ECaC1 and ECaC2. The two channels co-localize in calbindin-D-expressing tissues, including small intestine, pancreas and placenta, whereas kidney and brain express only ECaC1 and stomach solely ECaC2. From an electrophysiological point of view, the two channels are highly similar, with differences regarding the permeation properties and Ca^{2+}-dependent recovery of inactivation. A potentially important lead for the future is the differential sensitivity for ruthenium red of the channels, which makes the dissection of individual ECaC currents possible in tissues were the two channels are co-expressed.

Almers, W. & McCleskey, E. W. (1984). Non-selective conductance in calcium channels of frog muscle: calcium selectivity in a single-file pore. *Journal of Physiology* **353**, 585–608.

Barley, N. F., Howard, A., O'Callaghan, D., Legon, S. & Walters, J. R. F. (2001). Epithelial calcium transporter expression in human duodenum. *American Journal of Physiology* **280**, G285–290.

Caterina, M. J., Schumacher, M. A., Tominaga, M., Rosen, T. A., Levine, J. D. & Julius, D. (1997). The capsaicin receptor: a heat-activated ion channel in the pain pathway. *Nature* **389**, 816–824.

Delany, N. S., Hurle, M., Facer, P., Alnadaf, T., Plumpton, C., Kinghorn, I., Gee See, C., Costigan, M., Anand, P., Woolf, C. J., Crowther, D., Sanseau, P. & Tate, S. N. (2001). Identification and characterization of a novel human vanilloid receptor-like protein, VRL-2. *Physiological Genomics* **4**, 165–174.

Elsharyday, A., Syed, R., Tyagi, S., Khudeira, A. K., Harig, J. M. & Dudeja, P. K. (1995). Calcium transport mechanism in human colonic apical membrane vesicles. *Gastroenterology* **109**, 876–884.

Harteneck, C., Plant, T. D. & Schultz, G. (2000). From worm to man: three subfamilies of TRP channels. *Trends in Neurosciences* **23**, 159–166.

Hess, P., Lansman, J. B. & Tsien, R. W. (1986). Calcium channel selectivity for divalent and monovalent cations. Voltage and concentration dependence of single channel current in ventricular heart cells. *Journal of General Physiology* **88**, 293–319.

Hess, P. & Tsien, R. W. (1984). Mechanism of ion permeation through calcium channels. *Nature* **309**, 454–456.

Hoenderop, J. G. J., Müller, D., Suzuki, M., van Os, C. H. & Bindels, R. J. M. (2000*a*). Epithelial calcium channel: gate-keeper of active calcium reabsorption. *Current Opinion in Nephrology and Hypertension* **9**, 335–340.

Hoenderop, J. G. J., van der Kemp, A. W., Hartog, A., van de Graaf, S. F., van Os, C. H., Willems, P. H. G. M. & Bindels, R. J. M. (1999*a*). Molecular identification of the apical epithelial Ca^{2+} channel in 1,25-vitamin D_3 responsive epithelia. *Journal of Biological Chemistry* **274**, 8375–8378.

Hoenderop, J. G. J., van der Kemp, A. W., Hartog, A., van Os, C. H., Willems, P. H. G. M. & Bindels, R. J. M. (1999*b*). The epithelial calcium channel, ECaC, is activated by hyperpolarization and regulated by cytosolic calcium. *Biochemical Biophysical Research Communications* **261**, 488–492.

Hoenderop, J. G. J., Willems, P. H. G. M. & Bindels, R. J. M. (2000*b*). Toward a comprehensive molecular model of active calcium reabsorption. *American Journal of Physiology – Renal Physiology* **278**, F352–360.

Karbach, U. & Feldmeier, H. (1993). The cecum is the site with the highest calcium absorption in rat intestine. *Digistive Disease Science* **38**, 1815–1824.

Lepple-Wienhues, A. & Cahalan, M. D. (1996). Conductance and permeation of monovalent cations through depletion-activated Ca^{2+} channels (ICRAC) in Jurkat T cells. *Biophysical Journal* **71**, 787–794.

Liedtke, W., Choe, Y., Marti-Renom, M. A., Bell, A. M., Denis, C. S., Sali, A., Hudspeth, A. J., Friedman, J. M. & Heller, S. (2000). Vanilloid receptor-related osmotically activated channel (VR-OAC), a candidate vertebrate osmoreceptor. *Cell* **103**, 525–535.

Miller, S. A., Dykes, D. D. & Polesky, H. F. (1988). A simple salting out procedure for extracting DNA from human nucleated cells. *Nucleic Acids Research* **16**, 1215.

Müller, D., Hoenderop, J. G. J., Meij, I. C., van den Heuvel, L. P., Knoers, N. V., den Hollander, A. I., Eggert, P., Garcia-Nieto, V., Claverie-Martin, F. & Bindels, R. J. M. (2000*a*). Molecular cloning, tissue distribution, and chromosomal mapping of the human epithelial Ca^{2+} channel (ECAC1). *Genomics* **67**, 48–53.

Müller, D., Hoenderop, J. G. J., Merkx, G. F. M., van Os, C. H. & Bindels, R. J. M. (2000*b*). Gene structure and chromosomal mapping of human epithelial calcium channel. *Biochemical Biophysical Research Communication* **275**, 47–52.

Nadler, M. J., Hermosura, M. C., Inabe, K., Perraud, A. L., Zhu, Q., Stokes, A. J., Kurosaki, T., Kinet, J. P., Penner, R., Scharenberg, A. M. & Fleig, A. (2001). LTRPC7 is a Mg.ATP-regulated divalent cation channel required for cell viability. *Nature* **411**, 590–595.

Nilius, B., Prenen, J., Hoenderop, J. G. J., Bindels, R. J. M. & Droogmans, G. (2001*a*). Modulation of the epithelial calcium channel, ECaC, by intracellular Ca^{2+}. *Cell Calcium* **29**, 417–428.

Nilius, B., Prenen, J., Vennekens, R., Hoenderop, J. G. J., Bindels, R. J. M. & Droogmans, G. (2001*b*). Pharmacological modulation of monovalent cation currents through the epithelial Ca^{2+} channel ECaC1. *British Journal of Pharmacology* **134**, 453–462.

Nilius, B., Vennekens, R., Prenen, J., Hoenderop, J. G. J., Bindels, R. J. M. & Droogmans, G. (2000). Whole-cell and single channel monovalent cation currents through the novel rabbit epithelial Ca^{2+} channel ECaC. *Journal of Physiology* **527**, 239–248.

Nilius, B., Vennekens, R., Prenen, J., Hoenderop, J. G. J., Droogmans, G. & Bindels, R. J. M. (2001*c*). The single pore residue Asp542 determines Ca^{2+} permeation and Mg^{2+} block of the epithelial Ca^{2+} channel. *Journal of Biological Chemistry* **276**, 1020–1025.

Peng, J. B., Chen, X. Z., Berger, U. V., Vassilev, P. M., Brown, E. M. & Hediger, M. A. (2000*a*). A rat kidney-specific calcium transporter in the distal nephron. *Journal of Biological Chemistry* **275**, 28186–28194.

Peng, J. B., Chen, X. Z., Berger, U. V., Vassilev, P. M., Tsukaguchi, H., Brown, E. M. & Hediger, M. A. (1999). Molecular cloning and characterization of a channel-like transporter mediating intestinal calcium absorption. *Journal of Biological Chemistry* **274**, 22739–22746.

Peng, J. B., Chen, X. Z., Berger, U. V., Weremowicz, S., Morton, C. C., Vassilev, P. M., Brown, E. M. & Hediger, M.A. (2000*b*). Human calcium transport protein CaT1. *Biochemical and Biophysical Research Communications* **278**, 326–332.

Suzuki, M., Ishibashi, K., Ooki, G., Tsuruoka, S. & Imai, M. (2000). Electrophysiologic characteristics of the Ca-permeable channels, ECaC and CaT, in the kidney. *Biochemical and Biophysical Research Communications* **274**, 344–349.

Trouet, D., Nilius, B., Voets, T., Droogmans, G. & Eggermont, J. (1997). Use of a bicistronic GFP-expression vector to characterise ion channels after transfection in mammalian cells. *Pflügers Archiv* **434**, 632–638.

Vennekens, R., Hoenderop, J. G. J., Prenen, J., Stuiver, M., Willems, P. H. G. M., Droogmans, G., Nilius, B. & Bindels, R. J. M. (2000). Permeation and gating properties of the novel epithelial Ca^{2+} channel. *Journal of Biological Chemistry* **275**, 3963–3969.

Vennekens, R., Prenen, J., Hoenderop, J. G. J., Bindels, R. J. M., Droogmans, G. & Nilius, B. (2001*a*). Pore properties and ionic block of the rabbit epithelial calcium channel expressed in HEK 293 cells. *Journal of Physiology* **530**, 183–191.

Vennekens, R., Prenen, J., Hoenderop, J. G. J., Bindels, R. J. M., Droogmans, G. & Nilius, B. (2001*b*). Modulation of the epithelial Ca^{2+} channel ECaC by extracellular pH. *Pflügers Archiv* **442**, 237–242.

Vennekens, R., Trouet, D., Vankeerberghen, A., Voets, T., Cuppens, H., Eggermont, J., Cassiman, J. J., Droogmans, G. & Nilius, B. (1999). Inhibition of volume-regulated anion channels by expression of the cystic fibrosis transmembrane conductance regulator. *Journal of Physiology* **515**, 75–85.

Wadhwa, D. R. & Care, A. D. (2000). Effects of strontium on the absorption of calcium, magnesium and phosphate ions from the ovine reticulo-rumen. *Journal of Comprehensive Physiology* **170**, 225–229.

Yue, L., Peng, J. B., Hediger, M. A. & Clapham, D. E. (2001). CaT1 manifests the pore properties of the calcium-release-activated calcium channel. *Nature* **410**, 705–709.

Acknowledgements

J.G.J.H. was supported by a grant from EMBO (ALTL 160-2000) and D.M. was supported by the Deutsche Forschungsgemeinschaft (MU 1497 2-1). This study was supported in part by a grant from the Dutch Organization of Scientific Research (NWO-ALW 810-38-004). M. Crabbé, M. Schuermans and A. Janssens are acknowledged for their cell culture work. This work was supported in part by the Belgian Federal Government, the Flemish Government and the Onderzoeksraad KU Leuven (GOA 99/07, F.W.O.G.0237.95, F.W.O.G.0214.99, F.W.O.G.0136.00; Interuniversity Poles of Attraction Program, Prime Minister's Office IUAP Nr.3P4/23), 'Levenslijn' (7.0021.99) and a grant from the 'Alphonse and Jean Forton-Koning Boudewijn Stichting' (R7115 B0).

J. G. J. Hoenderop and R. Vennekens contributed equally to this study.

Corresponding author

R. J. M. Bindels: 160 Cell Physiology, University Medical Centre Nijmegen, PO Box 9101, NL-6500 HB Nijmegen, The Netherlands.

Email: reneb@sci.kun.nl